8

Micromechatronics

8.1 Modelling Micromechatronic Systems

8.1.1 Introduction

Micromechatronic or microelectromechanical systems (MEMS) represent a significant part of microsystem technologies. We will consider surface micromechanics as an example here, because in this field it is often possible to design the process steps for micromechanics to be compatible with those for microelectronics, which permits an integration of electronics and mechanics on a die. The dynamic interactions between electronics and mechanics often cannot be disregarded in such systems. Rather, the desired functionality is often only achieved by the close coupling between the domains. Furthermore, the natural frequencies of the mechanical and electronic oscillations often lie in the same range. This tends to be rare for the general case of an electro-mechanical system and is primarily associated with small mechanical component dimensions in the range of a few tens to a few hundreds of microns. With typical material parameters this yields mechanical resonance frequencies in the megahertz range. Thus a coupled simulation is a crucial prerequisite for the design of electro-mechanical microsystems.

A glance at the development of microelectronics over the last 20 years helps to characterise the situation. The availability of efficient simulation tools was a key factor for dynamic development of the integrated circuits. Precise and efficient models of basic components were, and remain, vital prerequisites for this. In the case of microelectronics only very few components, such as MOS transistors, diodes, capacitors or resistors, have to be taken into account. The introduction of micromechanics has changed matters. For MEMS a variety of nonelectrical components, with a still much greater number of geometric variations, have to be modelled, which leads to significant problems.

The modelling and simulation of MEMS can be considered on component or system level. In the first case, the emphasis is placed upon the design and optimisation of micromechanics, the second case focuses on how a micromechanical component behaves in the context of the system, i.e. within a circuit, for example,

Mechatronic Systems Georg Pelz
© 2003 John Wiley & Sons, Ltd ISBN: 0-470-84979-7

and how the entire system can be designed and optimised. The methods of the first category often form the basis for the consideration of the higher abstraction level.

8.1.2 Component design

A whole range of CAE methods have been proposed for the design of micromechanical components in recent years, see for example Funk *et al.* [108], Puers *et al.* [341], Sandmaier *et al.* [358] or Zhang *et al.* [436]. The MEMCAD system, described by Senturia *et al.* [381] provides a good example of this. Figure 8.1 shows an overview of the structure of this CAE system. In the first stage a so-called structure simulator is used in order to depict the descriptions of the mask layout and the process sequence provided by the user in the three-dimensional geometry of micromechanics, along with a process history for the selection of the appropriate materials. This is facilitated by the repeated call up of a lower-level process simulator. Whilst the geometry becomes a 3D model by meshing in finite elements or boundary elements, we can use the information of the process history to select the appropriate material parameters in the database. This is combined with the 3D model and can then be subjected to a mechanical or electrostatic analysis. Often such analyses should be coupled together, because the underlying phenomena, such as, for example, elasticity mechanics, inertia mechanics, electrostatics, or fluidics,[1] should be considered jointly. Two fundamental approaches have been

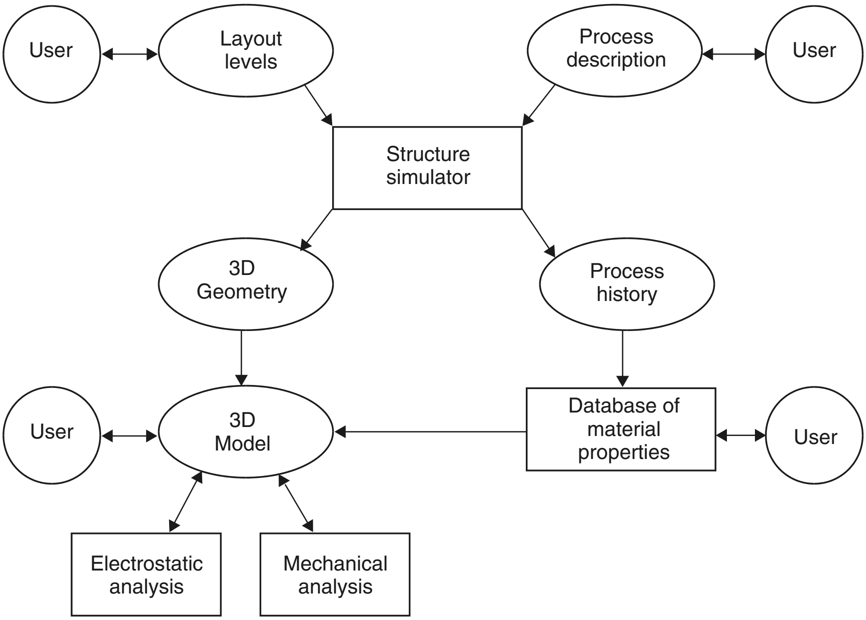

Figure 8.1 Structure of the MEMCAD system, see [381], for the design of MEMS

[1] For the description of damping of the mechanical movement in gases and fluids.

developed in recent years for the solution of this problem. Firstly, we can consider the various domains using coupled FE or BE simulators,[2] see, for example, Cai *et al.* [57], Gilbert *et al.* [119] or Senturia *et al.* [381]. The other possibility is to accommodate the various domains in *one* FE simulator on the basis of appropriate finite elements, such as, for example, in Funk *et al.* [108]. In the first case the participating simulators are called up sequentially until a state is reached that is both stable and also compatible with all domains. Such a state is also called self-consistent. In the other case, the analyses of the various domains within a simulator are iterated, with a self-consistent solution only being reached after a while.

In addition to the analysis of the predetermined design, the exploration of the design space is also supported in some cases. For example, Lee *et al.* [223] propose a technique called 'Design-Window', which replaces the single passage through all predetermined parameter combinations with a search led by a neural network. The number of iterations through automatic 3D modelling, meshing, and FE simulation operations run by the system, is thereby minimised.

8.1.3 System design

In contrast to the previous section, in system design the environment of the components has to be taken into account. In our context this is normally a circuit that either effects the triggering of a micromechanical actuator or the read-out of a micromechanical sensor.

Which models are suitable for describing the mechanics in a MEMS? A whole range of criteria can be drawn up here, which should ideally be fulfilled. In most cases, however, we are still a long way removed from this. In our context a mechanics model should:

- be sufficiently precise to correctly represent reality;
- be efficiently simulatable, so that the computing time remains within reasonable limits;
- not cause numerical problems;
- permit the setting of all significant design and technology parameters, in order to thus ensure the general applicability of the model;
- describe (quasi-)static and dynamic behaviour;
- be able to formulate the retention and dissipation of energy in relation to the application.

In addition, there is also the problem of determining the main material and technological parameters. Examples of these parameters are fabrication-related

[2] FE: finite elements, BE: boundary elements.

compressive or tensile stresses, the modulus of elasticity, or the dielectric constants. In some cases no values can be found in the literature. For example, the modulus of elasticity of polycrystalline silicon depends, amongst other things, upon its grain structure and its doping, and thus has to be determined individually for each case. This typically occurs on the basis of test structures, which are used for parameter extraction and are incorporated into process control, as in microelectronics, see for example Kiesewetter *et al.* [192] or Voigt *et al.* [415]. If no precise values can be provided here, the reliability of the simulation is jeopardised.

The two demonstrators represented in the following describe the structural modelling for a circuit simulator based upon finite elements. The first example relates to a capacitive pressure sensor in surface micromechanics, see Dudaicevs *et al.* [87] and [88]. The second example is an actuator in the form of a micromirror, which is arranged in an array on a chip, can be deflected individually, and in this manner generates pixel images for all types of displays, see Kück *et al.* [209], Younse [433] and Bielefeld *et al.* [29].

8.2 Demonstrator 5: Capacitive Pressure Sensor

8.2.1 System description

Using the approach described above, microsystems are investigated that cannot be described simply by the mass/spring/damper paradigms, i.e. nonsuspended systems. A good example for this is the integrated, capacitive pressure sensor system in surface micromechanics. Figure 8.2 shows a chip photo of such a system.

The fundamental principle[3] is based upon the fact that an external liquid or gas pressure bends the upper plate of the sensor element downwards, see Figure 8.3 and Figure 8.4. This leads to a change in the capacitance, which is detected by a read-out circuit. The system behaviour depends upon the elastic line of the plate, because it determines the capacitance of the arrangement. Consequently, the precise strain should be taken into account during an electro-mechanic simulation. In addition, the fact that the determination of the capacitance requires the application of a read-out voltage, which itself causes an electrostatic force between the plates, also gives rise to parasitic feedback. This again changes the deflection, which leads to a variation of the capacitance read.

The conversion of the capacitance into an output voltage is carried out in two stages using ‘switched capacitor’ technology. The first stage compares the sensor capacitance with a passivated reference capacitance. As a result of this differential processing, the result is barely influenced by manufacturing-related deviations. The second stage is the amplification of the read-out signal. Finally the output signal is smoothed by a ‘sample and hold’ stage. The circuit contains around 700 analogue components. The eighteen sensor and reference elements are each connected in

[3] See also the description in Section 6.3.3.

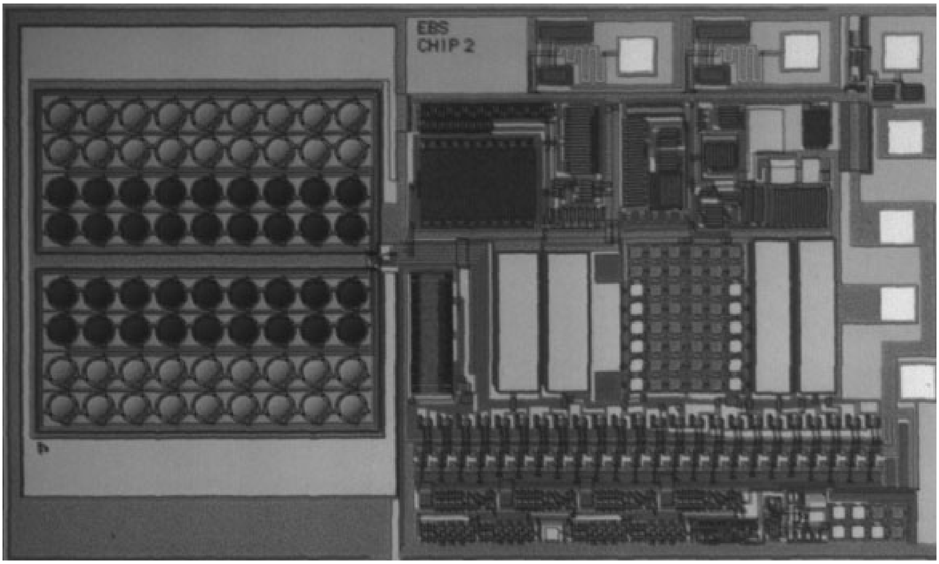

Figure 8.2 Chip photo of the integrated, capacitive pressure sensor system in surface micromechanics (Reproduced by Permission of Gerhard-Mercator-University, Duisburg, Germany)

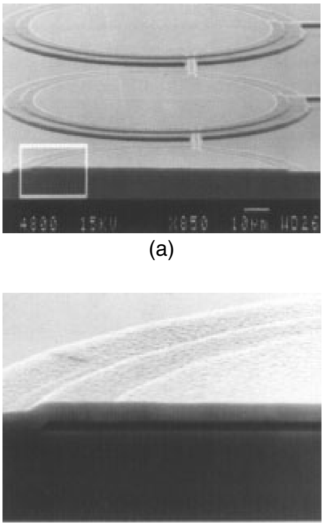

(a)

(b)

Figure 8.3 SEM photo of the cross-section of a pressure element (Reproduced by Permission of Fraunhofer-Institute IMS, Duisburg, Germany)

parallel. This array of eighteen active and eighteen passivated pressure elements, is duplicated in order to achieve still higher precision using differential path technology. For each set of eighteen pressure elements, a concentrated component is used, the capacitance of which is correspondingly multiplied.

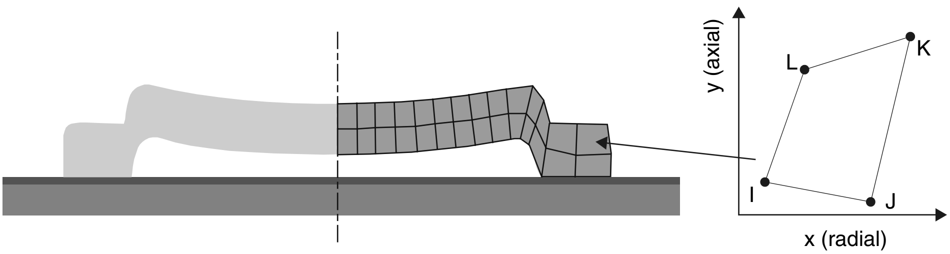

Figure 8.4 Arrangement of finite elements for the modelling of the micromechanical pressure element (left); plane element each with the degrees of freedom u and v per node (right)

The described system consists primarily of two sections: the conversion of pressure into capacitance and the read-out of the capacitance. Special emphasis lies on the investigation of the system behaviour. This means that we apply a pressure profile and consider the resulting voltage profile. In addition to the actual functionality, however, further properties of the sensor have to be investigated; for example, its sensitivity or linearity.

8.2.2 Modelling

Introduction

The circuit consists of the following components: 634 MOS field effect transistors, 52 resistors, 19 capacitors and 12 diodes. These components are either modelled in hardware description languages or permanently integrated into the simulator. We can generally rely upon the component models offered by the simulator here.

The modelling of the mechanics is more difficult, see also Pelz *et al.* [333] and Bielefeld *et al.* [33]. Two fields of 18 pressure elements each–one is passivated, the other is non-passivated–have to be considered. For modelling it is sufficient to describe one element each time and to multiply the capacitance values by 18. The passivated boxes can be simply replaced by a reference capacitance here because their capacitance deviation can be disregarded in this case.

The actual modelling of the pressure elements takes place by a radial section, which is justified by its rotationally symmetrical structure, see Figure 8.4. The section is described by a number of finite (plane) elements. In the simplest investigated case 28 elements are used, as illustrated. Each finite element has four nodes, each with two degrees of freedom, u and v, the deflection in the x and y directions. Multiplying the number of elements and the number of degrees of freedom of an element results in a total of 224 degrees of freedom. The actual number of degrees of freedom is significantly less, i.e. only 81. This is because many nodes of adjacent elements lie on one another, so that the degrees of freedom in question coincide.

The interpolation functions, and thus the element matrices, for the implementation of the plane element correspond with the solution selected in the FE simulator

ANSYS. Thus, as shown later in the simulation experiments, the mechanical behaviour cannot be distinguished from that simulated using ANSYS.

Setting up the element matrices

Now, the finite element to be formulated in a hardware description language should be parametrisable with regard to its dimensions and the associated material constants. Furthermore, the model should also be suitable for greater deflections. Both cases require that the element matrices must be constructed in the model of the finite elements. In this way the approach described here, see [333] and [33], differs significantly from the (later) work of Haase *et al.* [131] in which a system matrix of the mechanics constructed using a FE simulator is imported into a circuit simulator via a hardware description language.

The construction of the element matrices should be represented for an isoparametric, rotationally symmetrical plane element, see also Bathe [19]. For this purpose a natural coordinate system is introduced for the element, which has the coordinates s and t, which each run from −1 to +1 see Figure 8.5.

The first step is to approximate the coordinates of arbitrary points of the plane elements on the basis of the coordinates of the four nodes. To this end the form functions h_i are introduced, which are formulated as follows in the natural reference system of the element:

$$\begin{aligned} h_1 &= \tfrac{1}{4}(1-s)(1-t) \qquad h_2 = \tfrac{1}{4}(1+s)(1-t) \\ h_3 &= \tfrac{1}{4}(1+s)(1+t) \qquad h_4 = \tfrac{1}{4}(1-s)(1+t) \end{aligned} \tag{8.1}$$

The fundamental property of these functions is that the h_i becomes equal to 1 at node i and becomes equal to 0 at all other nodes.

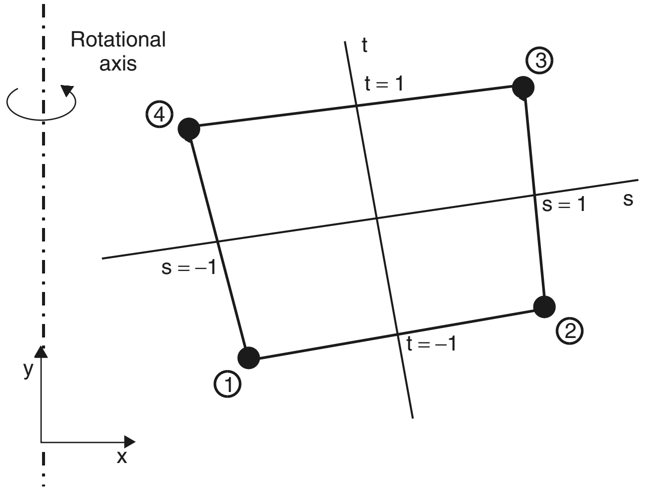

Figure 8.5 Natural coordinate system for a rotationally symmetrical plane element

The local coordinates of arbitrary points (x, y) of the element are thus found to be:

$$x = \sum_{i=1}^{4} h_i x_i, \qquad y = \sum_{i=1}^{4} h_i y_i \tag{8.2}$$

where x_i or y_i denote the coordinates of the element nodes. In the isoparametric formulation the element displacements are interpolated similarly to the coordinates, but this time the node displacements are multiplied by the form functions.

$$u = \sum_{i=1}^{4} h_i u_i, \qquad v = \sum_{i=1}^{4} h_i v_i \tag{8.3}$$

Here u and v are the local element displacements at an arbitrary point of the element and u_i and v_i are the corresponding element displacements at the nodes. The node displacements are furthermore summarised in the form of a vector:

$$\hat{\mathbf{u}}^T = \begin{bmatrix} u_1 & v_1 & u_2 & v_2 & u_3 & v_3 & u_4 & v_4 \end{bmatrix} \tag{8.4}$$

Thus (8.3) can be drawn up in matrix form:

$$\mathbf{u}(s, t) = \mathbf{H}\hat{\mathbf{u}} \tag{8.5}$$

The next step is the transition from the element displacements to the element strain $\boldsymbol{\varepsilon}$, which is defined by the derivative of the displacements with respect to the local coordinates:

$$\boldsymbol{\varepsilon}^T = \begin{bmatrix} \varepsilon_{xx} & \varepsilon_{yy} & \gamma_{xy} & \varepsilon_{zz} \end{bmatrix} = \begin{bmatrix} \frac{\partial u}{\partial x} & \frac{\partial v}{\partial y} & \frac{\partial u}{\partial y} + \frac{\partial v}{\partial x} & \frac{\partial w}{\partial z} \end{bmatrix} \tag{8.6}$$

The last entry of $\boldsymbol{\varepsilon}$ corresponds with the hoop strain, which is triggered by a displacement in the x-direction over the whole circumference according to the rotational symmetry.

We can thus draw up the strain-displacement transformation matrix **B**, which effects the transformation of the displacements to the strains.

$$\boldsymbol{\varepsilon} = \mathbf{B} \cdot \hat{\mathbf{u}}, \qquad \mathbf{B} = \begin{bmatrix} \frac{\partial h_1}{\partial x} & 0 & \frac{\partial h_2}{\partial x} & 0 & \frac{\partial h_3}{\partial x} & 0 & \frac{\partial h_4}{\partial x} & 0 \\ 0 & \frac{\partial h_1}{\partial y} & 0 & \frac{\partial h_2}{\partial y} & 0 & \frac{\partial h_3}{\partial y} & 0 & \frac{\partial h_4}{\partial y} \\ \frac{\partial h_1}{\partial y} & \frac{\partial h_1}{\partial x} & \frac{\partial h_2}{\partial y} & \frac{\partial h_2}{\partial x} & \frac{\partial h_3}{\partial y} & \frac{\partial h_3}{\partial x} & \frac{\partial h_4}{\partial y} & \frac{\partial h_4}{\partial x} \\ \frac{h_1}{R} & 0 & \frac{h_2}{R} & 0 & \frac{h_3}{R} & 0 & \frac{h_4}{R} & 0 \end{bmatrix} \tag{8.7}$$

where R is the radius relating to the rotation. The hoop strain is calculated as:

$$\frac{\partial w}{\partial z} = \frac{u}{R} \tag{8.8}$$

The element displacements u and v are, however, defined in the natural coordinate system (s,t), so that the derivatives with respect to x and y must be linked to the derivatives with respect to s and t. According to the chain rule, the following applies:

$$\begin{bmatrix} \partial/\partial s \\ \partial/\partial t \end{bmatrix} = \mathbf{J} \begin{bmatrix} \partial/\partial x \\ \partial/\partial y \end{bmatrix} \qquad \text{where} \quad \mathbf{J} = \begin{bmatrix} \partial x/\partial s & \partial y/\partial s \\ \partial x/\partial t & \partial y/\partial t \end{bmatrix} \tag{8.9}$$

It is a prerequisite that a clear relationship between the coordinate systems exists. In this case the following applies:

$$\begin{bmatrix} \partial/\partial x \\ \partial/\partial y \end{bmatrix} = \mathbf{J}^{-1} \begin{bmatrix} \partial/\partial s \\ \partial/\partial t \end{bmatrix} \tag{8.10}$$

By the use of the inverted Jacobi's operator $\mathbf{J}^{-1}$ we can now set up the strain vector for arbitrary points on the rotationally symmetrical plane elements.

We then move from the strains $\boldsymbol{\varepsilon}$ to the stresses $\boldsymbol{\tau}$, by using the material matrix **C**:

$$\boldsymbol{\tau} = \mathbf{C} \cdot \boldsymbol{\varepsilon} \qquad \text{where} \qquad \boldsymbol{\tau}^T = [\tau_{xx} \tau_{yy} \tau_{xy} \tau_{zz}] \tag{8.11}$$

For the material matrix of a rotationally symmetrical element the following applies according to [19]:

$$\mathbf{C} = \frac{E(1-\nu)}{(1+\nu)(1-2\nu)} \begin{bmatrix} 1 & \frac{\nu}{1-\nu} & 0 & \frac{\nu}{1-\nu} \\ \frac{\nu}{1-\nu} & 1 & 0 & \frac{\nu}{1-\nu} \\ 0 & 0 & \frac{1-2\nu}{2(1-\nu)} & 0 \\ \frac{\nu}{1-\nu} & \frac{\nu}{1-\nu} & 0 & 1 \end{bmatrix} \tag{8.12}$$

In the material matrix, E represents the modulus of elasticity and ν represents Poisson's ratio. To determine the stiffness matrix we first apply the elastic potential of a plane element:

$$\boldsymbol{\Pi} = \frac{1}{2} \int_A \boldsymbol{\varepsilon}^T \boldsymbol{\tau} \, dA \tag{8.13}$$

Alternatively we can also formulate

$$\boldsymbol{\Pi} = \frac{1}{2} \hat{\mathbf{u}}^T \mathbf{K} \hat{\mathbf{u}} \tag{8.14}$$

If we finally equate (8.13) and (8.14), then using (8.7) and (8.11) we find the following expression for the stiffness matrix:

$$\mathbf{K} = \int_A \mathbf{B}^T \mathbf{C} \mathbf{B} dA \tag{8.15}$$

Because the coordinates of the matrix **B** are defined in the natural coordinates, the integration must be performed using these coordinates

$$dA = \det \mathbf{J}\, ds\, dt \tag{8.16}$$

Substituting yields:

$$\mathbf{K} = \int_A \mathbf{F}\, ds\, dt \qquad \text{where} \qquad \mathbf{F} = \mathbf{B}^T \mathbf{C} \mathbf{B} \det \mathbf{J} \tag{8.17}$$

Since the analytical integration is difficult to get to grips with, at this point a numerical integration will be performed on the basis of the Gauss–Legendre quadrature. To this end the following support points are used in natural coordinates:

Support points (i,j)	s_i	t_j	α_{ij}
(1,1)	−0.577350269189626	−0.577350269189626	1.0
(1,2)	−0.577350269189626	+0.577350269189626	1.0
(2,1)	+0.577350269189626	−0.577350269189626	1.0
(2,2)	+0.577350269189626	+0.577350269189626	1.0

For every support point the matrix $\mathbf{F}_{ij}$ has to be evaluated and multiplied by the factor α_{ij}. The result is summed and forms the element stiffness matrix:

$$\mathbf{K} = \sum_{i,j} 2\pi R_{ij} \alpha_{ij} \mathbf{F_{ij}} \tag{8.18}$$

Here $\mathbf{F}_{ij}$ of the matrix corresponds with **F** at the integration points s_i and t_j. The values of α_{ij} are weighting factors that are determined for the numerical integration. Finally, the factor $2\pi R_{ij}$ represents the circumference with regard to the rotation at the integration point (s_i, t_j) and thus the ‘thickness’ of the element.

The creation of the element mass matrix is similarly completed in accordance with the equation:

$$\mathbf{M} = \int_A \rho \mathbf{H}^T \mathbf{H}\, dA \tag{8.19}$$

where ρ represents the material density and **H** the transformation matrix from (8.5). The above-mentioned operations are implemented in the programming language C.

This is based upon a library of matrix operations. As the following section shows, the C routines for element stiffness matrix and element mass matrix are called up from the hardware description, in order to determine the matrices in question. The above-mentioned operations for the creation of the element matrices should be performed at least once at the beginning of the simulation and several times in the event of greater deflections or nonlinearities.

Formulation in a hardware description language

The finite plane element called `plane_u2` described in the previous sections will now be formulated in an analogue hardware description language, see Hardware description 8.1. The MAST language has been selected for this. Two aspects have to be taken care of: the creation of the mass and stiffness matrices of the elements dealt with in the previous section and the linking of the mechanics thus described into a circuit simulation, see Chapter 6.

First of all the question of the terminals and parameters of the model arises. With its eight degrees of freedom the plane element should also possess eight terminals, which each represent one degree of freedom. These are deflections of the nodes i, j, k and l in the x and y directions, so the pins will be called `uxi, uyi, uxj, uyj, uxk, uyk, uxl` and `uyl`. With regard to the parameters, we differentiate between geometric and material parameters. The former specify the geometry of the element, i.e. the position of the nodes i, j, k and l in nondistorted state, and are called `xi, yi, xj, yj, xk, yk, xl` and `yl`. The latter are the density (dens), the modulus of elasticity in the x direction (`ex`) and y direction (`ey`), the shear modulus (`gxy`) Poisson's ratio (`nuxy`) and information about whether the element is to be considered as rotationally symmetrical (`plstr`).

There follows the declarations of the C routine (`foreign`), which calculates the element matrices, declarations of the element entries themselves (`l1_1, c1_1` ...) and the introduction of the branch (`branch`) that associates the value of internal variables with voltages and currents. In the following Values section the aforementioned C routine is called up in order to determine the element matrices. Depending upon the type of the finite element and application case, this may take place once at the beginning or as required during the simulation. Finally, the equation section includes the equation system that describes the element, in which each equation defines capacitive or inductive behaviour.

```
template plane_u2 uxi uyi uxj uyj    \
                  uxk uyk uxl uyl =  \
                  xi, yi, xj, yj,    \
                  xk, yk, xl, yl,    \
                  dens, ex, ey, gxy, \
                  nuxy, plstr
  electrical uxi,  # x-deflection, node i
             uyi,  # y-deflection, node i
      .....
  number xi = 0.0, # x-coordinate, node i
         yi = 0.0, # y-coordinate, node i
      .....
  number dens = 0.0, # Density
      .....
{
  foreign planeu2    # C function
      ....
  val nu l1_2,l1_3,l1_4, # L coefficient
      ....
         c1_1,c1_3,      # C coefficient
      ....
  # Definition of branch voltages and currents
  # at node uxi
  branch i1_1a = i(uxi->gnd), \
         v1_1 = v(uxi,gnd)
  ....
  ....
  # at node uyl
  branch i8_8a = i(uyl->gnd), \
         v8_8  = v(uyl,gnd)
  # Call up of the external C function for the calculation
  # of the mass and stiffness matrix of the element
  values{
    ...
    (l1_2,l1_3,......    \
     c1_1,c1_3,.....) =  \
    plane_u2 (xi, yi, .....)
    ...
  }
  # Definition of the dynamic equations
  equations{
    i1_1a = d_by_dt(v1_1  * c1_1)
    v1_2  = d_by_dt(i1_2b * l1_2)
    ....
    i8_8a = d_by_dt(v8_8  * c8_8)
    }
}
```

Hardware description 8.1 Description of the finite plane elements, each with four nodes and two degrees of freedom

System matrix

Using the element description obtained in this manner the deflections of the finite elements in question are represented by the voltages at the terminals of the element. The currents at the nodes in question describe the integral of the associated forces and moments, depending upon whether the degree of freedom relates to a translational or rotational deflection. In particular, the parts of the exciting forces and moments that are assigned to the elements adjoining the node are also added to the currents (and current changes) at a node. It is not necessary to explicitly create the system matrix, since its solution is yielded implicitly from the interconnection of the finite elements.

Excitation of the mechanics

In addition to the mechanical behaviour of the structure it is necessary to describe the external mechanical excitation. For reasons of modularity this is formulated in a further element, which is connected to the finite plane elements in question at the node(s) where the excitation acts. The main task of this element is to determine the exciting forces and moments at each node point, i.e. for each degree of freedom, and to convert these into a current change, with the resulting current being fed into the circuit nodes of the degree of freedom in question. The same procedure can in principle also be used in order to model the electrostatic feedback using an additional element. However, this effect could mainly be disregarded in the application considered, so that the corresponding modelling could be dispensed with.

Geometric nonlinearity

If the deflection exceeds a certain value, then the upper plate rests upon the isolator. If the pressure is further increased the plate ‘rolls’ out over the isolator. This corresponds with a one-sided holonomous and scleronomic constraint of the movement. Numerically this means that upon the manifestation of new boundary conditions, a corresponding number of degrees of freedom disappear. The realisation of numerical equation solvers with a variable number of unknowns or equations is a difficult task; only very few solvers are set up for this case. For this reason it is worthwhile approximating the prescribed situation by damping the specified degrees of freedom to a significant degree. This again leads to the fact that only minimal movements are possible for these, which in principle corresponds with the desired behaviour. However, this procedure may nevertheless be numerically dangerous because the sudden setting of a high damping — in other words the striking of the plate on the isolator — excites the most important natural frequencies.

Calculation of the capacitance

A further element type is introduced for calculating the capacitance, which just like the plane element or the pressure element is formulated in a rotationally symmetrical manner. For this element the plate capacitor equation is applied to the average deflection of a corresponding annulus. The resulting capacitance, in the form of variable capacitors, is positioned between the two plate potentials and is thus available to the circuit.

8.2.3 Simulation

In the following, various simulations will be performed in order to illustrate the application of finite elements for a circuit simulator. The following cases will be considered here: mechanical deflections, changes of the element capacitance, system simulation and the parametrised simulation of the FE models. A FE model of the sensor structure based upon 48 finite elements was used.

Mechanical behaviour

Initially the mechanical behaviour will be verified on the basis of a comparison with the FE simulator ANSYS. For this purpose three different element radii (120 μm, 70 μm and 50 μm) are predetermined and the deflection of various points on the radius considered, see Figures 8.6, 8.7 and 8.8. The results show virtually no differences between FE and the circuit simulator. This is because precisely the same interpolation functions, and thus element matrices, are used. Thus we lose no precision in relation to FE simulation. Such a simulation on the basis of hardware description languages requires around one CPU minute on a SUN Sparc 20 workstation.

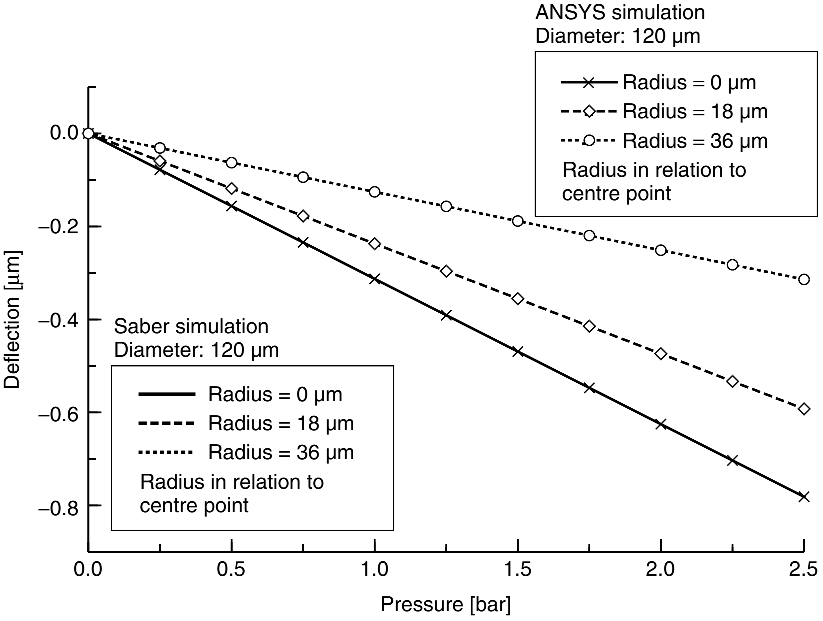

Figure 8.6 Mechanical deflection of the upper plate (diameter 120 μm) at various points on the radius. Comparison of the ANSYS FE simulator with the Saber circuit simulation

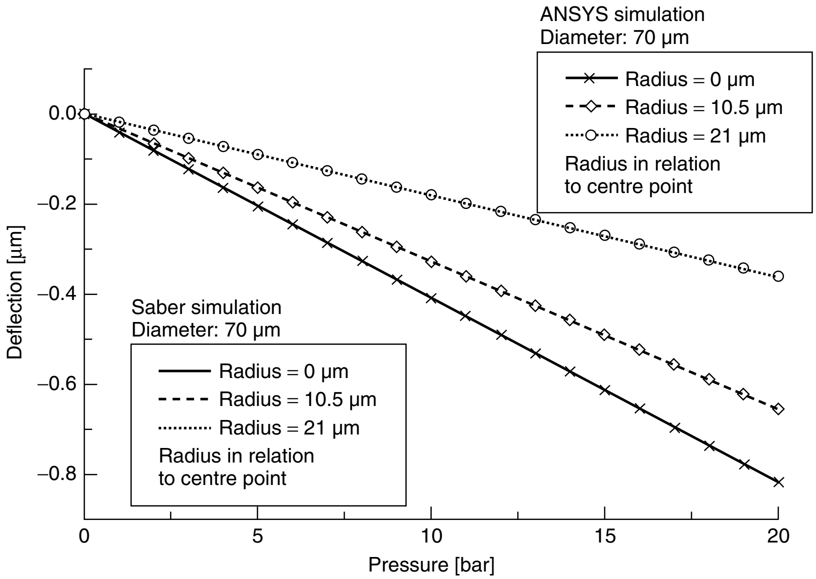

Figure 8.7 Mechanical deflection of the upper plate (diameter 70 µm) at various points on the radius. Comparison of the ANSYS FE simulator with the Saber circuit simulator

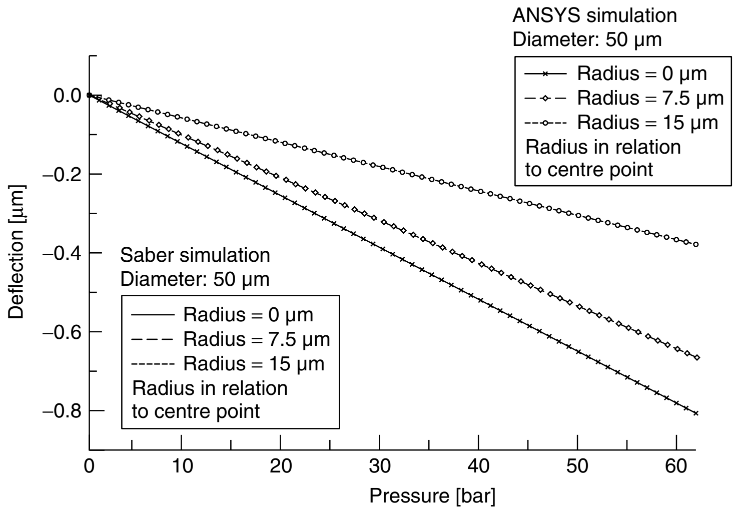

Figure 8.8 Mechanical deflection of the upper plate (diameter 50 µm) at various points on the radius. Comparison of the ANSYS FE simulator with the Saber circuit simulator

The mechanics was very slowly excited in the previous simulations and thus considered as quasi-static. In the modelling, however, the inertia was also specified, so that we can also investigate the kinetics in the simulation. This was taken into account in the following simulation, which shows the reaction of the mechanical structure to a sudden change of pressure, see Figure 8.9.

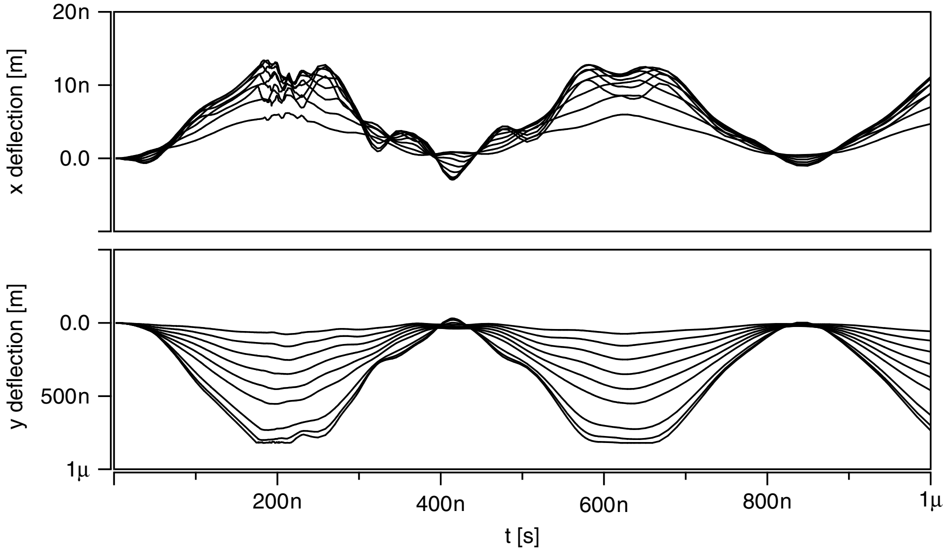

Figure 8.9 Response of the mechanical structure to a sudden change of pressure

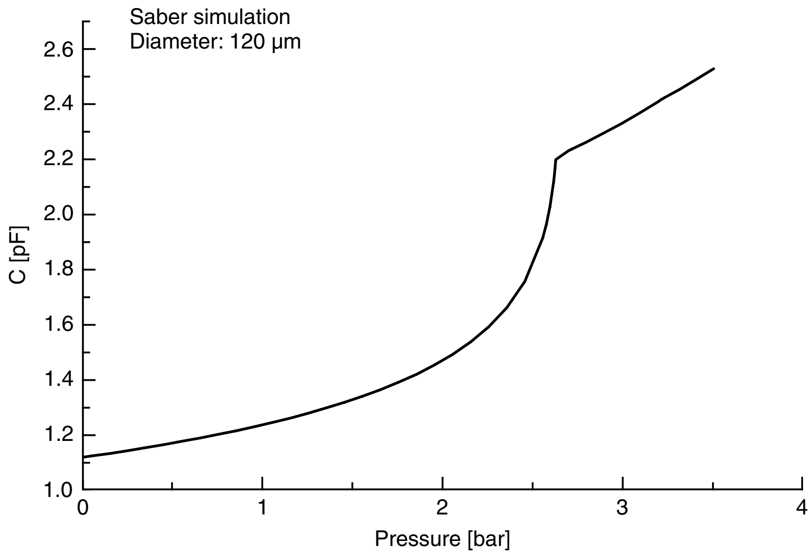

Figure 8.10 Capacitance against pressure for an element diameter of 120 μm

The x and y displacements of various points on the radius are considered, see for comparison Figure 8.4. The horizontal (x) displacements are positive and in the direction of the plate. They are smaller by a factor of 50 than the vertical (y) displacements, which have negative values and consequently describe a lowering of the plate. In a vertical deflection of −800 nm, the plate meets the isolator, which acts as a mechanical stop and thus causes a geometric nonlinearity. In particular, various natural frequencies are excited as a result of the collision, which is particularly evident from the displacement in the x-direction. It is clear that this type of simulation permits the consideration of the electro-mechanical dynamics in a transient simulation. Furthermore we can read off the most important natural frequencies from such a simulation.

Electrical behaviour

The electrical behaviour of the pressure elements is mainly connected to its capacitance. Figures 8.10, 8.11 and 8.12 show how the capacitance of an element behaves in relation to the pressure. This situation is considered on the basis of a transient simulation, in which the external pressure is increased in a linear manner. We note the kink in the curve, which marks the point at which the upper plate rests upon the isolator. If the pressure increases further the plate 'rolls' over the isolator and exhibits the typical, significantly more linear increase. Furthermore, regarding the various base capacitances at 0 bar, we note that arrays of 6, 18 and 33 pressure elements were selected for the diameters of 120, 70 and 50 μm respectively. The numbers selected correspond with a real fields used for pressure elements.

System simulation

In this section a transient simulation of the pressure sensor system shown in Figure 8.2 will be presented, see Figure 8.13. The applied pressure will be increased

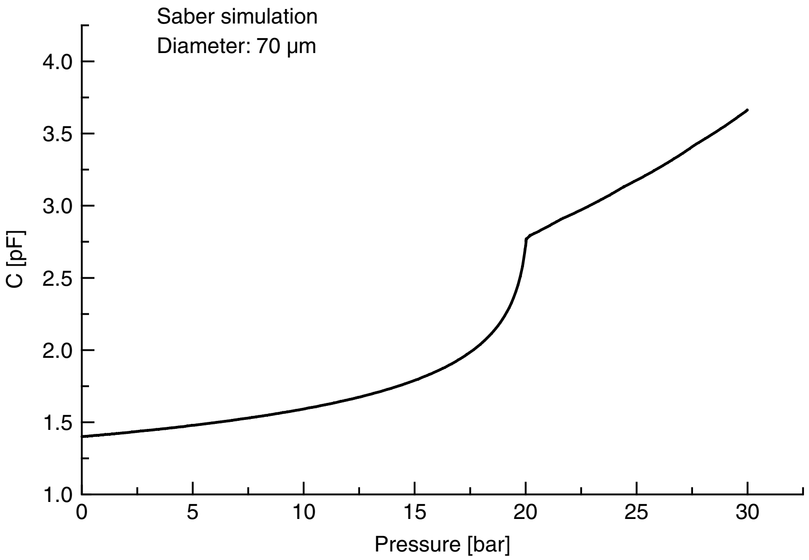

Figure 8.11 Capacitance against pressure for an element diameter of 70 μm

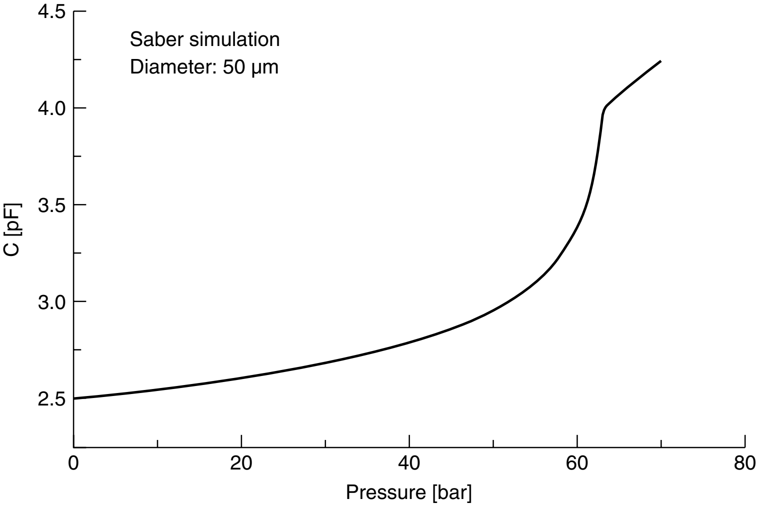

Figure 8.12 Capacitance against pressure for an element diameter of 50 μm

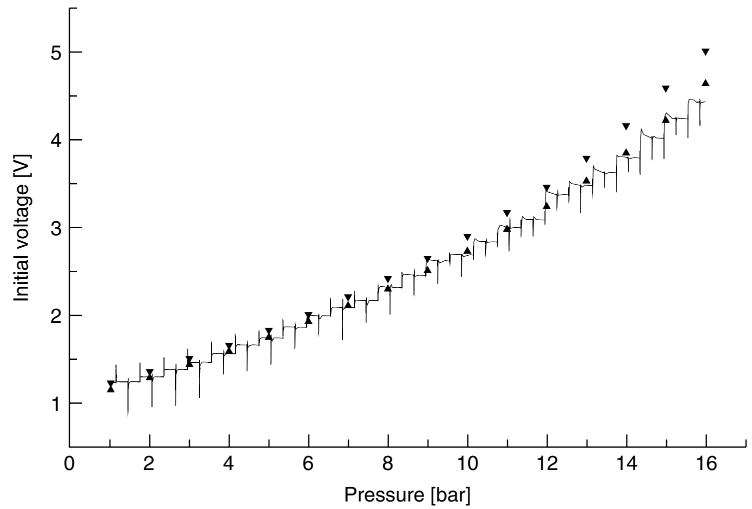

Figure 8.13 Output voltage against pressure for a pressure sensor system. Simulation (solid line), seven series of measurements, the maximum and minimum values of which are each marked by the triangles

continuously from 1 bar to 16 bar. This deflects the pressure element, the change in capacitance of which is converted into an output voltage by the switched capacitor circuit. The simulation (solid line) shows the slightly nonlinear path of measured output voltage. The voltage peaks that occur at regular intervals are caused by the read-out using switched capacitor circuit technology. For the validation of the simulation, seven series of measurements, taken on a corresponding number of manufactured circuits, were considered. The extreme values of these measurements are each depicted by the small triangles. The scatter between the measurements is caused by the scatter between the circuits. The simulation reflects the measured trace with an accuracy of below 10%. It also shows that the simulation remains a little behind the measurements at higher pressures and thus greater deflections. This effect could be caused by the stronger electrostatic forces of the read-out voltage at greater deflections, which are not taken into account in the model. Overall, this type of simulation permits the investigation of the overall function of the system, and also its sensitivity and linearity. This is accomplished even before manufacture. For the case shown, such a system simulation requires around 77 CPU minutes on a SUN Sparc 20.

Parametric simulations

In a circuit simulator it is normal to vary the models based upon parameters, in order to cover as broad an application spectrum as possible. Such parameters can be yielded from the geometry of the structure and from the material properties. A geometric parameterisation, such as the length or width of MOS transistors, can be achieved within certain limits even for FE models. In our case the following parameters were taken into account: diameter of the pressure element; plate thickness and height of the hollow area.

In addition, there are naturally also material properties, for example, the modulus of elasticity, Poisson's ratio or the dielectric constant. A circuit simulator offers the possibility of running certain simulations repeatedly and thus travelling through a predetermined parameter space. This will be performed for one design parameter and one technology parameter, namely for the element diameter and the plate thickness. The prerequisite for this type of simulation is that the geometry of the FE model is variably formulated. This is illustrated in Figure 8.14.

Two parametric simulations are shown in Figure 8.15 and Figure 8.16, in which the diameter and the plate thickness are varied. In this manner the FE model can be used both for design and also for technological optimisation, taking into account the circuit aspects.

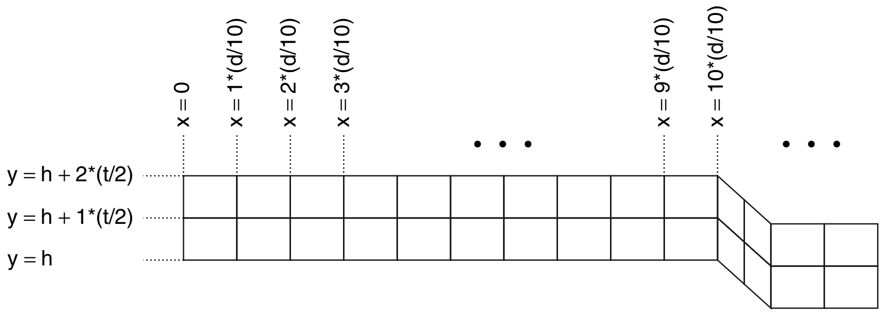

Figure 8.14 Geometric parameterisation of the FE model by diameter d, plate thickness t and height of the hollow space h

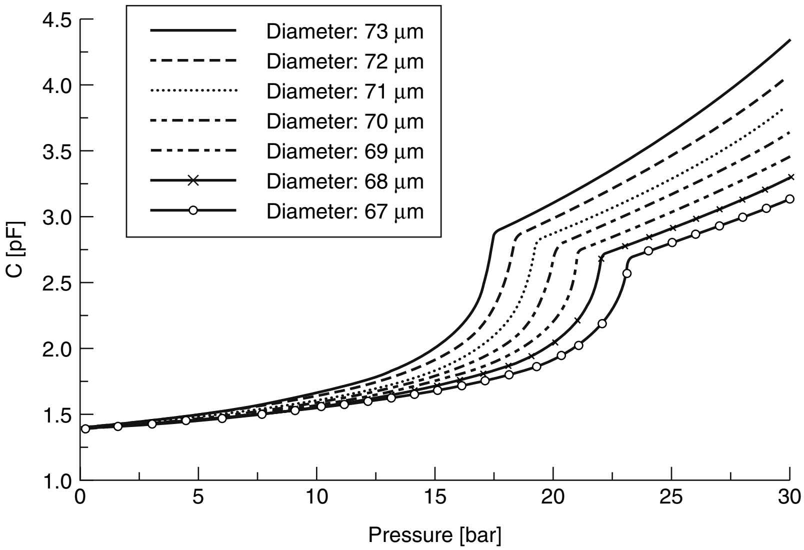

Figure 8.15 Parametric Saber simulations for the variation of the diameter of the pressure element. The plate thickness is fixed at 1.7 μm

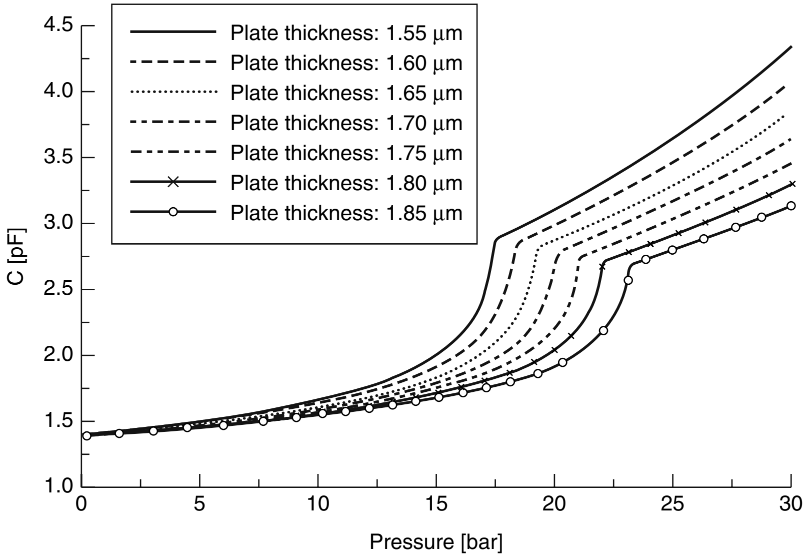

Figure 8.16 Parametric Saber simulations for the variation of the plate thickness of the pressure element. The diameter is fixed at 70 μm

8.3 Demonstrator 6: Micromirror

The second example here is a micromirror, which is arranged in arrays in order to generate pixel images of all types. Just like the pressure sensor described above, this micromirror, see Kück *et al.* [209], is a system manufactured using CMOS compatible surface micromechanics. It is operated as an actuator, i.e. the mechanical displacement is not the object of the measurement, but rather the system behaviour to be caused. Here the deflection consists of the lowering of the mirror. If light falls on the mirror its deflection brings about a corresponding phase shift in the reflected light. The picture to be generated finally arises from the resulting interferences. The deflection is achieved electrostatically.

8.3.1 System description

The micromirror has an edge length of 20 microns and is placed on the chip surface in large arrays, e.g. 512 × 464, see Figure 8.17.

Each mirror is individually addressable and can be moved independently of the others. The mirrors are deflected electrostatically by applying a suitable voltage between the mirror and a counter-electrode located below it. The restoring force of the suspension works against the electrostatic force, so the mirrors return to their initial positions after the voltage is switched off. One problem for modelling is that the resulting force depends significantly upon the distance between mirror and counter-electrode. In particular there is a positive feedback here, which can lead to instabilities.

8.3.2 Modelling

Due to the filigree structure of the micromirror, modelling cannot be achieved analytically without further complications. The finite element method is particularly suited to answering the questions of structural mechanics in such cases. Certain questions are essential to the consideration of the interaction between electronics

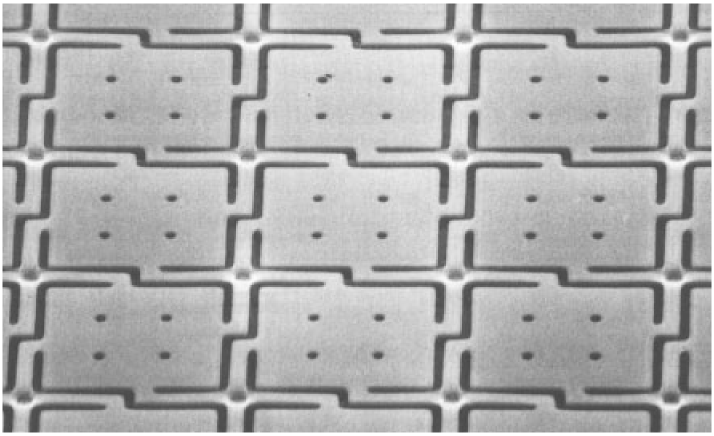

Figure 8.17 SEM photo of the micromirror layout (Reproduced by Permission of Fraunhofer-Institut IMS, Duisburg, Germany)

and mechanics. Initially the relationship between the voltage applied and the resulting deflection should of course be investigated. Furthermore, the feedback of the mirror capacitance on the electronics and the possible excitation of resonances of the mirror is also of interest. Figure 8.19 shows the typical deflection of a micromirror and the structure of the associated FE model. This is based upon plate elements, which are particularly well suited for the layer structure of micromechanics. The following representation deals with rectangular plate elements, which are treated in detail in Gasch and Knothe *et al.* [113]. The description of modelling is dealt with more briefly here in comparison with the previous demonstrator because — like the beams introduced in Chapter 6 — small deflections result in constant mass and stiffness matrices for the rectangular plate elements used. Furthermore, the customisation of the element matrices according to geometric and material parameters is very simple in this case.

Each element has four nodes, which lie at the corners of the plate element, see Figure 8.18. Each node again has four degrees of freedom (u_z, r_x, r_y, r_{xy}), where u_z represents the displacement perpendicular to the plane of the plate, r_x and r_y the cross-sectional tiltings in the x and y direction, and r_{xy} the torsion:

$$r_x = -\frac{\partial u_z}{\partial x}, \qquad r_y = -\frac{\partial u_z}{\partial y}, \qquad r_{xy} = -\frac{\partial^2 u_z}{\partial x \partial y} \tag{8.20}$$

The interpolation functions for the rectangular plate element can be obtained in an elegant manner by the multiplication of pairs of interpolation functions of a beam, see for example equation (6.35). One interpolation function covers the x-direction, the other the y-direction. If there are four interpolation functions for a beam there are sixteen interpolation functions for the plate. Using the principle of the virtual displacements we obtain a mass matrix and a stiffness matrix for the plate element, see [113]. The mass matrix depends exclusively upon the density of the material ρ and the dimensions of the plate, see equation (8.21). The stiffness matrix is again influenced by the dimensions, the modulus of elasticity of the material, and Poisson's ratio. In both cases 16 × 16 matrices are obtained which — as shown

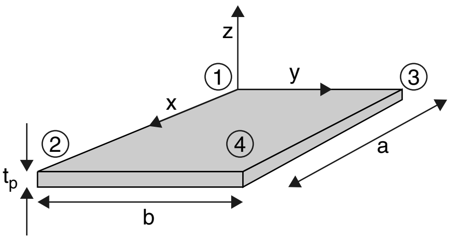

Figure 8.18 Finite element of a rectangular plate with four nodes and four degrees of freedom per node

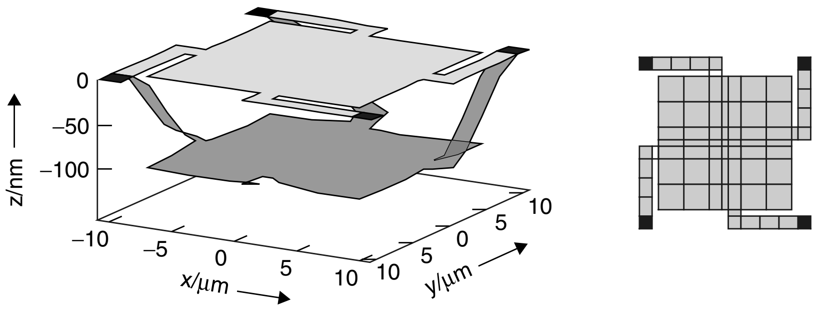

(a)

(b)

Figure 8.19 Deflection of a micromirror (a), structure of the FE model (b)

in Section 6.3.2–will be represented in hardware description languages.

$$
\mathbf{M} = \frac{\rho \mathrm{t_p ab}}{176400}
$$

$$
\times \begin{bmatrix}
24336 & 8424 & 8424 & 2916 & -3432 & 2028 & -1188 & 702 & -3432 & -1188 & 2028 & 702 & 484 & -286 & -286 & 169 \\
8424 & 24336 & 2916 & 8424 & -2028 & 3432 & -702 & 1188 & -1188 & -3432 & 702 & 2028 & 286 & -484 & -169 & 286 \\
8424 & 2916 & 24336 & 8424 & -1188 & 702 & -3432 & 2028 & -2028 & -702 & 3432 & 1188 & 286 & -169 & -484 & 286 \\
2916 & 8424 & 8424 & 24336 & -702 & 1188 & -2028 & 3432 & -702 & -2028 & 1188 & 343 & 169 & -286 & -286 & 484 \\
-3432 & -2028 & -1188 & -702 & 624 & -468 & 216 & -162 & 484 & 286 & -286 & -169 & -88 & 66 & 52 & -39 \\
2028 & 3432 & 702 & 1188 & -468 & 624 & -162 & 216 & -286 & -484 & 169 & 286 & 66 & -88 & -39 & 52 \\
-1188 & -702 & -3432 & -2028 & 216 & -162 & 624 & -468 & 286 & 169 & -484 & -286 & -52 & 39 & 88 & -66 \\
702 & 1188 & 2028 & 3432 & -162 & 216 & -468 & 624 & -169 & -286 & 286 & 484 & 39 & -52 & -66 & 88 \\
-3432 & -1188 & -2028 & -702 & 484 & -286 & 286 & -169 & 624 & 216 & -468 & -162 & -88 & 52 & 66 & -39 \\
-1188 & -3432 & -702 & -2028 & 286 & -484 & 169 & -286 & 216 & 624 & -162 & -468 & -52 & 88 & 39 & -66 \\
2028 & 702 & 3432 & 1188 & -286 & 169 & -484 & 286 & -468 & -162 & 624 & 216 & 66 & -39 & -88 & 52 \\
702 & 2028 & 1188 & 3432 & -169 & 286 & -286 & 484 & -162 & -468 & 216 & 624 & 39 & -66 & -52 & 88 \\
484 & 286 & 286 & 169 & -88 & 66 & -52 & 39 & -88 & -52 & 66 & 39 & 16 & -12 & -12 & 9 \\
-286 & -484 & -169 & -286 & 66 & -88 & 39 & -52 & 52 & 88 & -39 & -66 & -12 & 16 & 9 & -12 \\
-286 & -169 & -484 & -286 & 52 & -39 & 88 & -66 & 66 & 39 & -88 & -52 & -12 & 9 & 16 & -12 \\
169 & 286 & 286 & 484 & -39 & 52 & -66 & 88 & -39 & -66 & 52 & 88 & 9 & -12 & -12 & 16
\end{bmatrix} \tag{8.21}
$$

A total of 69 finite elements are used for the modelling of the micromirror, which are connected together as shown on the right-hand side of Figure 8.19. Ninety six nodes have to be considered, with four degrees of freedom each — thus a total of 384 degrees of freedom. In addition to the finite elements of the mechanics, further elements are used to calculate and apply an appropriate force from the applied voltage and the current deflection for each node. Further details with regard to modelling can also be found in Bielefeld *et al.* [34].

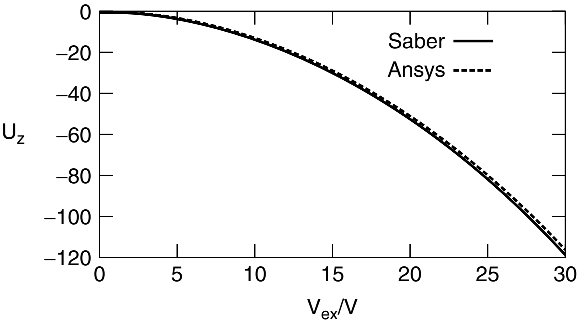

Figure 8.20 Simulation result: deflection of the mirror against the excitation potential; finite elements in hardware description languages (Saber) versus finite elements in a FE tool (ANSYS)

8.3.3 Simulation

In the quasi-static simulation shown in Figure 8.20 the excitation voltage increases linearly from 0 V to 30 V. The deflection of the micromirror is plotted against time or voltage. The results that were achieved using the Saber circuit simulator and the ANSYS FE simulator (at the same discretisation) are shown. The differences between the two simulations are below 2%, so the model formulated in hardware description languages can serve as a good replacement for the FE model. Both simulations require about a minute of CPU time on a SUN Sparc 20 workstation.

8.4 Summary

For virtually all FE simulators it is true that electronic components cannot be included in the simulation to an appreciable degree. So for these tools the consideration of the electronics goes no further than the formulation of electrostatic forces. By contrast, the point of the implementation of the finite elements using hardware description languages is that all models present in the electronics simulator can also be drawn into such a simulation. Thus the development of the electronics can be achieved taking into account continuum mechanics.

This is illustrated by the two demonstrators of this chapter. Both of these are microsystems. Nonetheless, exactly the same methodology is applicable for continuum mechanics of macro scale. We considered a sensor and an actuator, which can both be investigated equally well using the approach.